2014 IEEE International Conference on Robotics & Automation (ICRA)
Hong Kong Convention and Exhibition Center
May 31 - June 7, 2014. Hong Kong, China

Low-Friction Tendon-Driven Robot Hand with Carpal Tunnel Mechanism in the Palm by Optimal 3D Allocation of Pulleys

Tanut Treratanakulwong, Hiroshi Kaminaga and Yoshihiko Nakamura[1]

***Abstract*— Underactuated hands usually have high adaptability in power grasping but they are limited in pinching task with fingertip. In this paper, we propose the design of a tendon-driven underactuated hand that is capable of fingertip pinching by utilizing our proposed coupling mechanism. To reduce the friction resulting from tendon routing, we introduce the carpal tunnel mechanism that replace all sliding-contact tendon routing with the pulley system allocated in 3-dimensional space. The prototype of 11-DOF anthropomorphic robot hand is fabricated using rapid prototyping. Experiments are done to prove the effectiveness of our proposed coupling mechanism and low-friction tendon-driven system for underactuated robot hand.**

I. INTRODUCTION

A hand is one of the extremities that plays an important role in grasping and manipulation. A human hand is capable of holding heavy objects as well as performing dexterous movements, such as, playing piano. These capabilities of the human hand come from powerful muscles and huge numbers of degree of freedom (DOF). Considering a simplified model of a human hand, one finger has 4 DOFs, 3 DOFs for flexion-extension and 1 for abduction-adduction. One 5-fingered hand would contain at least 20 DOFs. This large number of DOFs contributes to the dexterous movements of the hands and the fingers. Each DOF in Gifu Hand [1] and HPR3 Hand [2] is driven with a small electric motor that can be fit inside the finger. DLR Hand [3] has joint torque sensors to sense the contact forces and perform a soft grasping. The main limitation of having all motors inside the hand is a weak output power. To make use of larger motors, [4] moves motors outside of the hand to the forearm and controls fingers using tendons. DLR Hand Arm System [5] has the number of actuators double the number of DOFs. By connecting elastic elements with the tendons, mechanical stiffness of each joint can be controlled independently.

Tendon driven mechanisms are beneficial in the sense that designers can separate the allocation of the actuators and the joint outputs which is desirable in the manipulator because smaller the link inertia, faster the response it is. A tendon routing need to be designed carefully so that friction remains as low as possible. However, the complexity of tendon routing increases as the number of tendons raise. One possible solution is to design the robot hand with the least number of DOFs to accomplish most of the grasping tasks. This can be done by learning the finger coordination from human grasping, so called "Synergies" [6][7]. Synergies dramatically reduce >20 DOFs of actuation to a couple DOFs, for example, 4 DOFs can regenerate 90% of the grasping pattern[8].

Underactuation enables the hand and fingers to adapt their shapes to the objects. USC/Belgrade Hand [6] is one example where joints are coupled with rigid links. Catalano et al. [9] develops a synergy-driven underactuated robot hand with elastic elements. Despite high adaptability, underactuated hands often suffer from object ejection in pinch grasping tasks.

In this paper, we propose an underactuated tendon-driven hand with pinch grasping capability. The proposed robot hand has 19 joints with 11 DOFs controlled by 12 tendons. The complex tendon-routing problem is formulated as an optimization problem of a pulley allocation in 3-dimensional space. We fabricated a 5-finger hand prototype using rapid prototyping technology where such a complex tendon-driven mechanism cannot be realized with conventional material-removal machining process.

II. DESIGN OF 4 FINGERS

None of the fingers in one hand are identical. Due to the physical differences in length, human uses each of them for a different purpose. We classify 4 fingers (excluding a thumb) into 2 groups. First, index and middle finger are prominent in pinching tasks and they are more powerful compared to the other two. Ring and little finger are used to increase a grasping stability. All four fingers share the common joint structure where each finger has 3 joints. The one closest to the palm is metacarpal joint (MCP) which is 2-DOF joint. In this paper, we name abduction-adduction joint as MCP1 and flexion-extension joint as MCP2. The middle joint is called proximal interphalangeal joint (PIP) and the most distal one is distal interphalangeal joint (DIP).

Index finger and Middle finger In human, we observe a coupling behaviour between PIP and DIP joint, due to an existence of a Retinacular ligament [10]. Human can flex MCP joint independently of the other two. Most of the underactuated hands [9][11][12]

*This work was supported by Research Grant-in-Aid for Scientific Research (S) (No.20220001) of the Japan Society for the Promotion of Science.

[1]T. Treratanakulwong, H. Kaminaga, and Y. Nakamura are with Graduate School of Information Science and Technology, The University of Tokyo, 7-3-1 Hongo, Bunkyo-Ku, Tokyo 113-8656, Japan. {tanut,kaminaga,nakamura}@ynl.t.u-tokyo.ac.jp

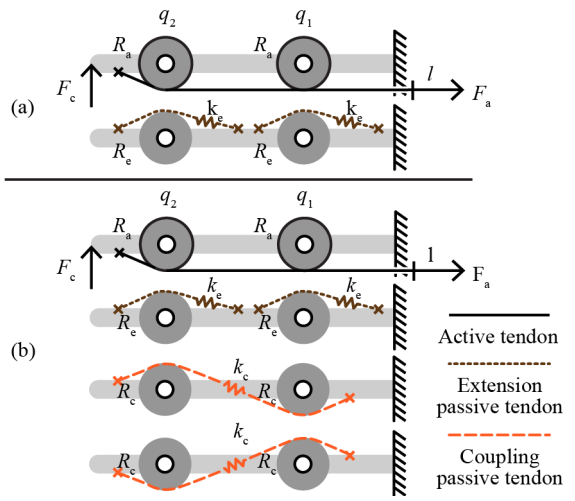

Fig. 1. Tendon routing of the conventional underactuated hand (a), and our proposed coupling for underactuated hand (b).

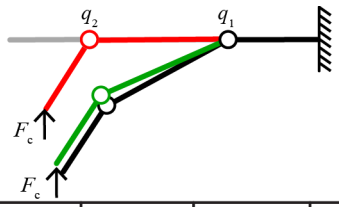

System setup	Coupling type	Contact Force (N)	Actuation Force (N)	Equilibrium Configuration
(a)	others (k_e=1)	F_c=0	F_a=0.00	
(b)	our (k_c,k_e=1)	F_c=0	F_a=0.00	
(c)	others (k_e=1)	F_c=0	F_a=0.50	
(d)	our (k_c,k_e=1)	F_c=0	F_a=0.50	
(e)	others (k_e=1)	F_c=1	F_a=1.54	
(f)	others (k_e=5)	F_c=1	F_a=3.49	
(g)	our (k_c,k_e=1)	F_c=1	F_a=1.49	

Fig. 2. Joint equilibrium configuration of each system setup.

have similar tendon configurations as shown in Figure 1(a). The design complexity is reduced because two joints are driven by one active tendon (the tendons controlled by actuator). Two passive tendons (spring or elastic bands) are added on the other side of the joints to create extension torques. Object ejection becomes a major problem of underactuated hand especially in a pinching task with fingertip. To prevent that behaviour, L. A. Demers et al. proposes to add another active tendons with a specific transmission ratio [13]. Since adding active tendons are costly, we proposed to reduce object ejections by redesigning the coupling mechanism with passive tendons instead of the active ones. Our proposed design is shown in Figure 1(b). We denote $\boldsymbol{q} = (q_1, q_2)^T$ as a joint configuration and derive the joint stiffness matrix of each design as follows,

$$K_{\mathrm{qa}} = \begin{pmatrix} R_{\mathrm{e}}^2 k_{\mathrm{e}} & 0 \\ 0 & R_{\mathrm{e}}^2 k_{\mathrm{e}} \end{pmatrix} \tag{1}$$

$$K_{\mathrm{qb}} = \begin{pmatrix} 2R_{\mathrm{c}}^2 k_{\mathrm{c}} + R_{\mathrm{e}}^2 k_{\mathrm{e}} & -2R_{\mathrm{c}}^2 k_{\mathrm{c}} \\ -2R_{\mathrm{c}}^2 k_{\mathrm{c}} & 2C^2 k_{\mathrm{c}} + R_{\mathrm{e}}^2 k_{\mathrm{e}} \end{pmatrix} \tag{2}$$

where K_{qa} is a joint stiffness matrix of the conventional system (Figure 1(a)) and K_{qb} for our proposed system (Figure 1(b)). Extension passive tendons (brown lines) have stiffness k_{e} and moment arm R_{e}. Coupling passive tendons are drawn in orange with the stiffness k_{c} and moment arm R_{c}. To compare these two systems, we assume a pinching situation where there is a constant contact force $\boldsymbol{F}_{\mathrm{c}}$ at the position $\boldsymbol{y} = \boldsymbol{c}$ and active tendon is pulled with tension F_{a} at the displacement l. The dynamic equation of fingers can be written as follows,

$$\mathcal{A}(\boldsymbol{q})\ddot{\boldsymbol{q}} + \mathcal{B}(\boldsymbol{q}, \dot{\boldsymbol{q}}) + \mathcal{C}\dot{\boldsymbol{q}} - \frac{\partial U(\boldsymbol{q})}{\partial \boldsymbol{q}} = \boldsymbol{0} \tag{3}$$

$$U(\boldsymbol{q}) = U_{\mathrm{g}}(\boldsymbol{q}) + U_{\mathrm{e}}(\boldsymbol{q}) + \lambda_1 h + \lambda_2 i \tag{4}$$

where

$$h = R_{\mathrm{a}} q_1 + R_{\mathrm{a}} q_2 - l = 0 \tag{5}$$

$$i = \boldsymbol{y} - \boldsymbol{c} = 0 \tag{6}$$

$\mathcal{A}(\boldsymbol{q})$, $\mathcal{B}(\boldsymbol{q},\dot{\boldsymbol{q}})$, and $\mathcal{C}$ are inertia matrix, torque due to the Coriolis and centrifugal forces, and coefficient matrix of dissipation which is assumed to be positive definite. The potential function $U(\boldsymbol{q})$ can be expressed as a combination of gravitational potential $U_{\mathrm{g}}(\boldsymbol{q})$, elastic potential $U_{\mathrm{e}}(\boldsymbol{q})$, the active wire constraint h with Lagrange multiplier λ_1, and contact force constraint i with multiplier λ_2. The total system converges to an equilibrium of the potential function by the proof of Takegaki-Arimoto paper [14].

To illustrate the numerical example of the equilibrium configuration $\boldsymbol{q}$, we substitute $R_{\mathrm{a}}, R_{\mathrm{c}}, R_{\mathrm{e}}, k_{\mathrm{c}}, k_{\mathrm{e}}, l$ with 1, F_{c} is either 0 or 1. K is either K_{qa} or K_{qb} depending on the system setups. Numbers are selected for simplicity but the property can be shown without the loss of generality. A forward kinematic of each solution is shown in Figure 2. When there is no contact force the proposed coupling behaves the same way as the others coupling (Figure 2(a)-(d)). However, when there is a contact force our proposed coupling deviate less from the case without contact force (Figure 2(g)). For the conventional design, large K_{c} is necessary to achieve the same equilibrium which results in larger actuation force F_{a} (Figure 7(f)). If larger actuation force is required to stabilize the same contact force, the system becomes less efficient.

A similar design of the coupling mechanism is proposed by Ozawa et al. [15]. In their implementation, extension is done by active tendons while passive tendons in our case. Doing so, we can further reduce the number of active tendons, resulting in less actuation complexity.

A conceptual tendon routing of MCP2, PIP, and DIP joint is shown in Figure 3. Since every active tendons' pulleys have the same radius, an extension passive tendon of the MCP2 must have the stiffness at least $2k_{\mathrm{e}}$ to let MCP2 be controlled independently of PIP and DIP.

Ring finger and Little finger help to constrain and support the grasped objects. Ring finger is implemented with one active tendon for flexion, 3 passive tendons for extension and the proposed coupling mechanism for 3 joints, shown in Figure 4. The most common design

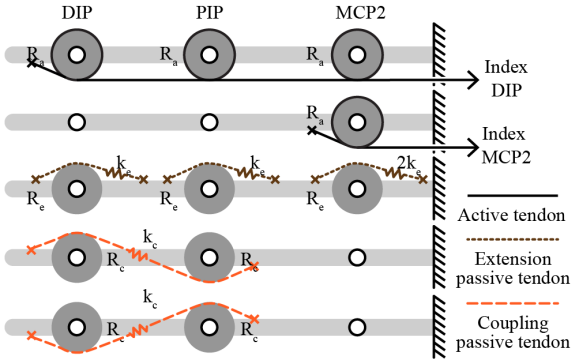

Fig. 3. Tendon routing of index and middle finger.

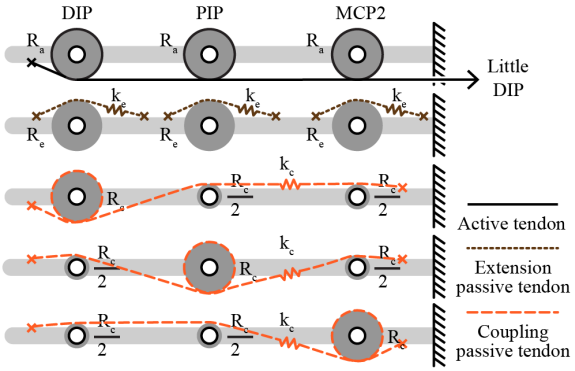

Fig. 4. Tendon routing of ring and little finger.

of 3-joint coupling is simply two of a 2-joint-coupling, MCP2/PIP and PIP/DIP. The main disadvantage of this design is that MCP2 and DIP are not coupled directly. Our proposed design of a 3-joint-coupling is based on the least number of constraints required for 3 joints which is 3 tendons. Pulley sizes vary depending on each constraint. Underactuation is still feasible because constraints are implemented by passive tendons. By using a similar technique to prove the joint equilibrium configuration as previously presented, it is possible to show that the proposed design is superior to the conventional design in pinching task with fingertip.

III. DESIGN OF THE THUMB

Opposition is a movement which a pulp of the thumb is facing to other fingers. Human thumb has wider range of opposition compared to other primates [10]. In grasping, the opposing thumb allows exerting contact forces on the opposite direction of the other fingers to create a force closure. To achieve a high dexterity of the thumb, all 4 joints must be controlled independently. Therefore, we designed the thumb with fully-actuated tendon-driven mechanism. Considering a mechanism with n_{w} tendons and n_{j} joints, we can express the relation between the velocity of tendons $\dot{\boldsymbol{x}} \in R^{n_{\mathrm{w}}}$ and the angular velocity of joints $\dot{\boldsymbol{q}} = (\dot{q_1}, \ldots, \dot{q_{n_{\mathrm{j}}}})^T \in \boldsymbol{R}^{n_{\mathrm{j}}}$ as follows,

$$\dot{\boldsymbol{x}} = J\dot{\boldsymbol{q}} \tag{7}$$

where $J \in R^{n_{\mathrm{w}} \times n_{\mathrm{j}}}$ is the Jacobian matrix of joint velocities and linear velocity of tendons. We can calculate the tension on each tendon $\boldsymbol{f}$ for a given arbitrary value of joint torques $\boldsymbol{\tau}$ as the following equation.

$$\boldsymbol{f} = -{J^{\#}}^T \boldsymbol{\tau} + N\boldsymbol{\xi} \tag{8}$$

$J^{\#}$ represents a pseudoinverse of the Jacobian matrix J. A null space N is represented by an arbitrary vector $\boldsymbol{\xi}$. The characteristic of tendon-driven mechanism is that tendons can transmit only positive tensions which infers that $\boldsymbol{f} \geq \boldsymbol{0}$ is a necessary condition for any tendon-driven system. As a consequence, $\boldsymbol{\xi}$ must exist. Therefore, the least number of tendons required to control n_{j}-DOF tendon-driven manipulator is $n_{\mathrm{j}} + 1$ tendons. For the 4-DOF thumb, at least 5 tendons are necessary to perform independent joint torque control. In fact, not every tendon routing is applicable, so we find such a tendon routing that permits full-controllability by optimization of tendon routing. Given a distinct tendon configuration denoted by $\mathcal{P}$, we can rewrite the Equation 8 as follows,

$$\boldsymbol{\tau} = J(\mathcal{P})^T(\boldsymbol{f} + \boldsymbol{f}_{\mathrm{b}}(\mathcal{P})) \tag{9}$$

where $J(\mathcal{P})$ is the Jacobian matrix of the tendon routing $\mathcal{P}$ and $\boldsymbol{f}_{\mathrm{b}}(\mathcal{P})$ is the bias force that lies in the null space of $J(\mathcal{P})^T$, denoted by $\mathrm{Null}(J(\mathcal{P})^T)$. $\boldsymbol{f}_{\mathrm{b}}(\mathcal{P}) > \boldsymbol{0}$ is a necessary condition to maintain positive tension forces for any joint torque configurations. A relatively good tendon routing $\mathcal{P}$ must has the bias force $\boldsymbol{f}_{\mathrm{b}}(\mathcal{P})$ as uniform as possible because actuators are assumed to have the same force capability. We defined $\boldsymbol{e} = 1/\sqrt{n_{\mathrm{w}}}(1, 1, \ldots, 1)^T$ as a n_{w}-dimensional uniform vector. We apply the following optimization to find good tendon-routing candidates.

$$\begin{aligned} \underset{\mathcal{P}}{\text{maximize}} \quad & \boldsymbol{e}^T \frac{\boldsymbol{f}_{\mathrm{b}}(\mathcal{P})}{|\boldsymbol{f}_{\mathrm{b}}(\mathcal{P})|} \\ \text{subject to} \quad & \boldsymbol{f}_{\mathrm{b}}(\mathcal{P}) > \boldsymbol{0} \text{ and } \boldsymbol{f}_{\mathrm{b}}(\mathcal{P}) \in \mathrm{Null}(J(\mathcal{P})^T) \end{aligned} \tag{10}$$

We also imposed the constrain on sizes of the pulleys to facilitate the implementation, and locations where tendons are terminated. The resulting tendon routing of the thumb is shown in Figure 5.

Human's thumb has slightly inclined joint axes to increase the pulp contact surfaces during the opposition [16]. Similar ideas can be found in the guideline to design robot hands [17]. In our implementation, we also twist the joint axes little by little to improve the overall grasping quality.

IV. PALM: LOW-FRICTION TENDON GUIDING

Flexor and extensor muscles are located inside forearm, called extrinsic muscles. Motions are transmitted to the finger joints by tendons. Flexor tendons are almost parallel to each other when they go through the wrist. Tendons' direction is controlled by carpal bones that form a carpal tunnel on a palmar side of the hand. Sheaths, as in Bowden cables, prevent tendons from

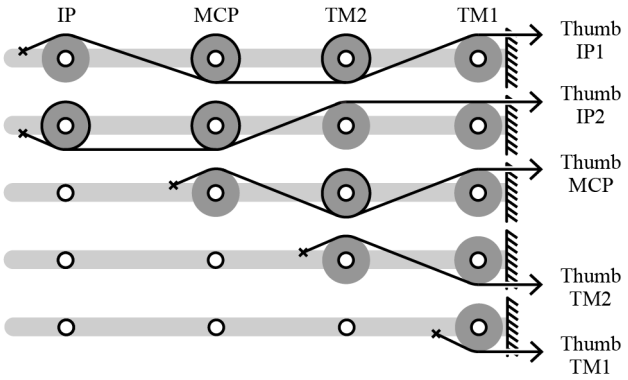

Fig. 5. An optimized tendon routing of the thumb that has 4 DOFs driven by 5 tendons.

colliding with the bones [10]. The main issue in designing a robot hand's palm is how to route the tendon with the lowest amount of friction. Friction does not only reduce a transmission efficiency (resulting in less grasping forces) but it also reduces the force controllability of the system. One of the early work in reducing friction is presented in Utah/MIT hand where the complex routing of tendon was solved by replacing tendons with flat belts [4]. Recently, highly underactuated hands suffer less from the tendon routing problem because the hand is usually driven by only few numbers of active tendons [9] while in the case of fully actuated robot hand, a tendon routing with sliding-contact is still unavoidable [5].

A tendon routing problem, in general, is the problem of changing tendons' direction from arbitrary input directions to any output directions. Several tendon-driven robot hands use Bowden cables [18] or low-friction plastic bushes to route the tendons. Even though a very low friction material is used, a sliding friction (PTFE $\mu \approx 0.05$) is relatively larger compared to a rolling friction ($\mu \approx 0.001$) of ball bearing [19]. For any two arbitrary input/output directions and positions, at least 2 pulleys are necessary to control the direction of the tendons. Once the routing of tendons is decided, we can build a structure that supports the specific positions and orientations of pulleys and shafts. The only remaining question is how to compute a tendon routing for multiple tendons under a given geometric constraint.

Considering n-th tendon, constraints on an input direction and output direction are given by the structure of the hand. m-th constraint is classified into two types.

1) Line constraint is defined by a linear equation in 3D-space where a contact point between tendon and routing pulley ($\boldsymbol{p}_m$) must be on the line defined by the following equation,

$$\boldsymbol{p}_m = \boldsymbol{a}_m + x_m \hat{\boldsymbol{u}}_m \tag{11}$$

where $\boldsymbol{a}_m$ is an entry point of the tendon, $\hat{\boldsymbol{u}}_m$ is a unit vector that represents tendon's direction, and $x_m \in [x_{m,\min}, x_{m,\max}]$ is a parameter that defines the location of that pulley with respect to the point $\boldsymbol{a}_\mathrm{m}$. This type of constrain is applied to all tendons from 4 fingers and one tendon from the thumb (Thumb TM1).

2) Plane constraint is interpreted as a plane of idler pulley where an angle θ_m of the tendon can be varied as well as a distance between idler pulley and the pulley$_m$. A contact point $\boldsymbol{p}_m$ between pulley$_m$ and the tendon can be calculated as,

$$\boldsymbol{p}_m = \boldsymbol{a}_m + x_m \mathrm{R}(\theta_m, \boldsymbol{n}_m)\hat{\boldsymbol{u}}_m \tag{12}$$

where $\boldsymbol{a}_m$ is the center of the idler pulley, $\hat{\boldsymbol{u}}_m$ is a unit vector that represents the direction of an entry tendon, and $\mathrm{R}(\theta_m, \boldsymbol{n}_m)$ is the rotation matrix around vector $\boldsymbol{n}_m$ that points along the axis of idler pulley. There are two free parameters that define $\boldsymbol{p}_m$ which are an angle $\theta_m \in [\theta_{m,\min}, \theta_{m,\max}]$ and the distance from idler pulley to the m-th pulley $x_m \in [x_{m,\min}, x_{m,\max}]$. This type of constrain is applied to all idler pulleys on the wrist and 4 tendons from the thumb.

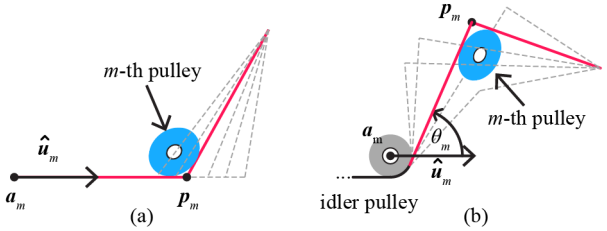

Fig. 6. Two types of constraints applied to all tendons in the optimization. Line constraint (a) and Plane constraint (b).

For a given set of parameters $\boldsymbol{x} = (x_1, \ldots, x_m)^T$ and $\boldsymbol{\theta} = (\theta_1, \ldots, \theta_m)^T$, it is possible to find the position ($\boldsymbol{c}_m$) and orientation ($\boldsymbol{n}_m$) for each routing m-th pulley. To find the best tendon routing that allows physical implementation, we optimize a cost function as shown in Equation 13. The first term expresses the cost of collision between any pair of pulleys that are closer than the smallest bounding sphere r_t centered at $\boldsymbol{c}_m$. The second term adds a penalty to the solution where any pairs of pulleys are far apart to make the design compact. The optimization problem of tendon routing can be formulated as follows,

$$\begin{aligned} \underset{\boldsymbol{x},\boldsymbol{\theta}}{\text{minimize}} \quad & \sum_{i \neq j} \frac{1}{\mathrm{dist}(c_i(\boldsymbol{x},\boldsymbol{\theta}), c_j(\boldsymbol{x},\boldsymbol{\theta}))} \\ & + \alpha(\mathrm{dist}(c_i(\boldsymbol{x},\boldsymbol{\theta}), c_j(\boldsymbol{x},\boldsymbol{\theta})) - r_\mathrm{t}) \\ \text{subject to} \quad & \boldsymbol{x} \in [\boldsymbol{x}_{\min}, \boldsymbol{x}_{\max}] \text{ and } \boldsymbol{\theta} \in [\boldsymbol{\theta}_{\min}, \boldsymbol{\theta}_{\max}] \end{aligned} \tag{13}$$

where $c_i(\boldsymbol{x},\boldsymbol{\theta}), c_j(\boldsymbol{x},\boldsymbol{\theta})$ are the center of pulley i, j of the tendon routing $\boldsymbol{x},\boldsymbol{\theta}$ and α is a weighting factor which is equal to 0.01 for the current calculation. We run the optimization with various initial points of $\boldsymbol{x},\boldsymbol{\theta}$ to find several candidates for the implementation.

The results are shown in Figure 7. The solution (c), (d), and (f) are not suitable for the implementation because some pulleys are on the same plane which makes the assembly difficult. Among the others we chose (e) because a distribution of pulleys and tendons is the most uniform. Pulleys' locations $\boldsymbol{c}_\mathrm{m}$ and axis orientation

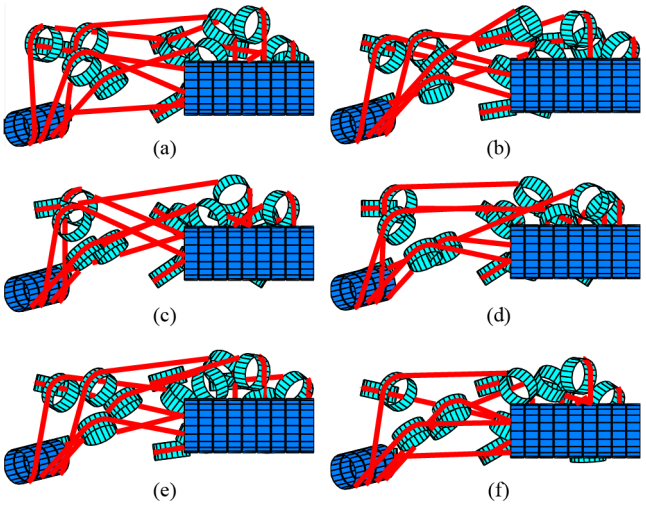

Fig. 7. Optimization result of tendon routing with various initial parameter $\boldsymbol{x}, \boldsymbol{\theta}$ (seeing from the wrist).

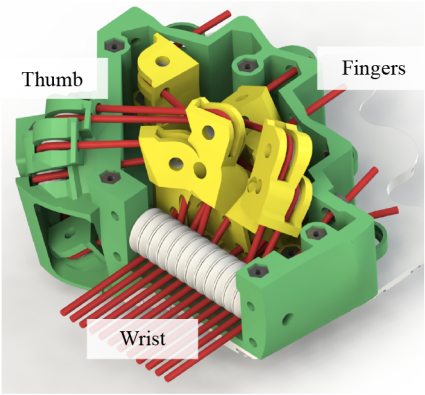

Fig. 8. Rendering of a pulley supporting structure inside the palm. Tendons from fingers are routed with 3D-pulley system before becoming parallel at the wrist.

$\boldsymbol{n}_{\mathrm{m}}$ are imported into computer aided design software (CAD). A 3D-pulley supporting structure are designed and validated to make sure that shaft holes and pulley slots are accessible from outside of the shape, otherwise the structure would become impossible to assemble. The final design of the pulley supporting structure is shown in Figure 8.

V. PROTOTYPE AND EXPERIMENTS

A prototype of five-fingered hand is fabricated by using Fused Deposition Modelling (FDM) 3D printer. Our design also exploits the uses of 3D printer because some parts cannot be built with the conventional material removal process, for example, the pulley-supporting structure inside the palm (Figure 8). The prototype hand consists of 19 joints, and 11 DOFs which are driven by 12 linear actuators. A back surface of the hand has curvatures that mimic the human hand for both cosmetic purpose and stress distribution (Figure 9(a)). Figure 9(b) shows arches created by the thumb and four other fingers. Palmar side of the hand prototype is covered with silicone skin which is made by insert-casting technique. A soft skin help to increase a grip, see Figure 9(c).

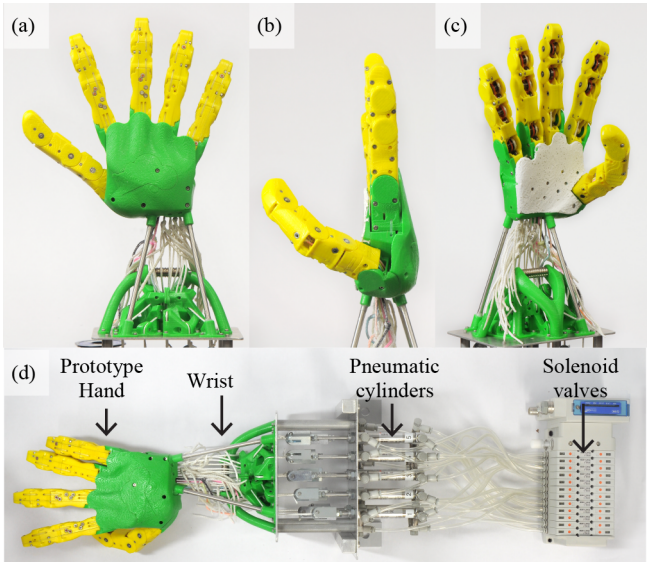

Fig. 9. Hand prototype (a) back side, (b) lateral side, (c) palmar side, (d) experiment setup with pneumatic actuators.

The design is intended to connect with the currently developing Electro-Hydrostatic Actuators (EHAs) cluster for robot hand [20] but for this demonstration, 12 active tendons are driven with 12 pneumatic cylinders which are controlled by dual three-way solenoid valves. The communication between a host computer and the solenoids is done over EtherCAT®. Figure 9(d) illustrates an experiment setup of the prototype hand with pneumatic actuators. The demonstration of each DOF and grasping are shown in the attached video.

We install 12-bit absolute magnetic encoder on every joints to study the behaviour of underactuated hand in grasping. Circuit boards and signal cables are enclosed inside the hand structure. In the first experiment, finger freely moves with no contact forces. An active tendon is pulled and joint angles are recorded and plotted against the actuator stroke, see Figure 10. In the case of index finger, only Index DIP tendon is pulled. PIP and DIP joint trajectory track a theoretical line where q_{DIP} is always equal to q_{PIP}. After the joint limits are reached, MCP2 joint started to move.

Three flexion joints of a little finger are coupled with the proposed 3-joint coupling mechanism. Therefore, MCP2, PIP, and DIP joint angles are almost at the same value. However, after the active tendon is released, we can observe a hysteresis which is supposed to come from pulley friction and friction between finger and elastic bands.

To confirm an underactuated capability of the proposed design, we fix the position of active tendon and apply external forces in various magnitude and orientations. Joint configurations are recorded and plotted with blue dots on Figure 11. White dots are the equilibrium configuration of a given actuator stroke when there is no contact forces. It can be seen from both graphs that blue dots stay close to the theoretical plane of underactuation

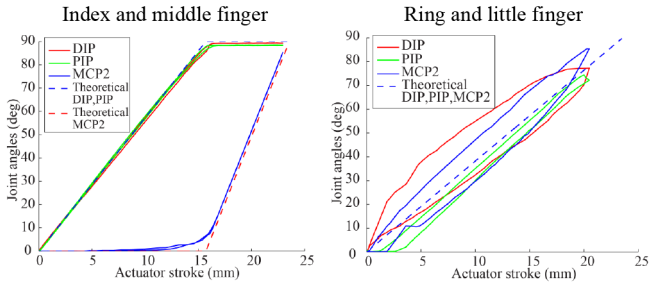

Fig. 10. Joint trajectory of index finger and little finger when there is no contact forces exerted on the finger.

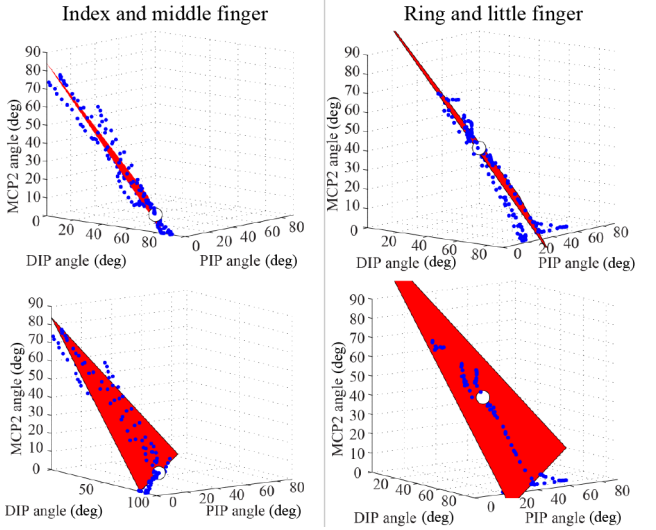

Fig. 11. Underactuation behaviour of index finger and little finger when actuator position is fixed and external forces are applied on the finger.

(red planes) which is imposed by the active tendon constraint. Plots on top and bottom row are from the same dataset but looking from the different viewpoint.

VI. CONCLUSION

In this paper, we presented the design of 11-DOF underactuated anthropomorphic hand. Coupling mechanism for underactuated hand is redesigned to reduce the object ejection. A friction from the tendon routing is significantly reduced by introducing a pulley system oriented in 3D-space that has purely rolling contact. A complex component inside the palm is a result of the optimization of tendon routing. Our design also exploits the benefit of 3D-printing fabrication. The prototype hand has 19 joints driven by 12 active tendons and weighted around 340 grams. Size and shape of the hand prototype are similar to the human hand (110 mm wide at the widest part, and 193 mm from the wrist to the fingertip of the middle finger). The prototype hand is driven by pneumatic cylinders to demonstrate its capability. The effectiveness of proposed coupling mechanism and low-friction tendon routing is demonstrated and discussed.

REFERENCES

[1] H. Kawasaki, T. Komatsu, and K. Uchiyama, "Dexterous anthropomorphic robot hand with distributed tactile sensor: Gifu hand II," *IEEE/ASME Transactions on Mechatronics*, vol. 7, no. 3, pp. 296–303, Sep 2002.

[2] K. Kaneko, K. Harada, F. Kanehiro, G. Miyamori, and K. Akachi, "Humanoid robot HRP-3," in *proc. of IEEE/RSJ International Conference on Intelligent Robots and Systems*, 2008, pp. 2471–2478.

[3] J. Butterfaß, M. Grebenstein, H. Liu, and G. Hirzinger, "DLR-Hand II: Next generation of a dextrous robot hand," in *proc. of IEEE International Conference on Robotics and Automation*, vol. 1, 2001, pp. 109–114.

[4] S. Jacobsen, E. Iversen, D. Knutti, R. Johnson, and K. Biggers, "Design of the Utah/M.I.T. dextrous hand," in *proc. of IEEE International Conference on Robotics and Automation*, vol. 3, 1986, pp. 1520–1532.

[5] M. Grebenstein, A. Albu-Schaffer, T. Bahls, M. Chalon, O. Eiberger, W. Friedl, R. Gruber, S. Haddadin, U. Hagn, R. Haslinger *et al.*, "The DLR hand arm system," in *proc. of IEEE International Conference on Robotics and Automation*, 2011, pp. 3175–3182.

[6] G. A. Bekey, R. Tomovic, and I. Zeljkovic, "Control architecture for the Belgrade/USC hand," in *Dextrous robot hands*. Springer, 1990, pp. 136–149.

[7] M. Gabiccini, A. Bicchi, D. Prattichizzo, and M. Malvezzi, "On the role of hand synergies in the optimal choice of grasping forces," *Autonomous Robots*, vol. 31, no. 2-3, pp. 235–252, 2011.

[8] C. Y. Brown and H. H. Asada, "Inter-finger coordination and postural synergies in robot hands via mechanical implementation of principal components analysis," in *proc. of IEEE/RSJ International Conference on Intelligent Robots and Systems*, 2007, pp. 2877–2882.

[9] G. Grioli, M. Catalano, E. Silvestro, S. Tono, and A. Bicchi, "Adaptive synergies: an approach to the design of under-actuated robotic hands," in *proc. of IEEE/RSJ International Conference on Intelligent Robots and Systems*, 2012, pp. 1251–1256.

[10] I. Kapandji, *The physiology of the joints*, ser. The Physiology of the Joints. Churchill Livingstone, 2008, no. v. 3. [Online]. Available: http://books.google.co.jp/books?id=k5wTAQAAMAAJ

[11] L. Wang, J. DelPreto, S. Bhattacharyya, J. Weisz, and P. K. Allen, "A highly-underactuated robotic hand with force and joint angle sensors," in *proc. of IEEE/RSJ International Conference on Intelligent Robots and Systems*, 2011, pp. 1380–1385.

[12] A. M. Dollar and R. D. Howe, "Joint coupling design of underactuated hands for unstructured environments," *The International Journal of Robotics Research*, vol. 30, no. 9, pp. 1157–1169, 2011.

[13] L.-A. A. Demers and C. Gosselin, "Kinematic design of an ejection-free underactuated anthropomorphic finger," in *proc. of IEEE International Conference on Robotics and Automation*, 2009, pp. 2086–2091.

[14] M. Takegaki and S. Arimoto, "A new feedback method for dynamic control of manipulators," *Journal of Dynamic Systems, Measurement, and Control*, vol. 103, no. 2, pp. 119–125, 1981.

[15] R. Ozawa, K. Hashirii, and H. Kobayashi, "Design and control of underactuated tendon-driven mechanisms," in *proc. of IEEE International Conference on Robotics and Automation*, 2009, pp. 1522–1527.

[16] A. Hollister, W. L. Buford, L. M. Myers, D. J. Giurintano, and A. Novick, "The axes of rotation of the thumb carpometacarpal joint," *Journal of Orthopaedic Research*, vol. 10, no. 3, pp. 454–460, 1992.

[17] M. Chalon, M. Grebenstein, T. Wimbock, and G. Hirzinger, "The thumb: Guidelines for a robotic design," in *proc. of IEEE/RSJ International Conference on Intelligent Robots and Systems*, 2010, pp. 5886–5893.

[18] Shadow Robot Company, "The shadow dexterous hand," http://www.shadowrobot.com/products/dexterous-hand/.

[19] B. Silliman, *Principles of Physics, Or Natural Philosophy*. Philadelphia : Theodore Bliss, 1871.

[20] T. Y. Kang, H. Kaminaga, and Y. Nakamura, "Design of an actuator cluster with casting cylinder and throchoid crest hydraulic pump for robot hand," in *31st Annual Conf. of* The Robotics Society Of Japan, 2013.